Applied Catalysis B: Environmental 156–157 (2014) 428–437

Contents lists available at ScienceDirect

Applied Catalysis B: Environmental

journal homepage: www.elsevier.com/locate/apcatb

In situ DRIFTS and temperature-programmed technology study on NH_3-SCR of NO_x over Cu-SSZ-13 and Cu-SAPO-34 catalysts

Lei Ma[a,b], Yisun Cheng[c], Giovanni Cavataio[c], Robert W. McCabe[c], Lixin Fu[a], Junhua Li[a,*]

[a] State Key Joint Laboratory of Environment Simulation and Pollution Control, School of Environment, Tsinghua University, Beijing 100084, China
[b] Department of Chemistry, Tsinghua University, Beijing 100084, China
[c] Research and Innovation Center, Ford Motor Company, Dearborn, MI 48121, USA

ARTICLE INFO

Article history:
Received 13 January 2014
Received in revised form 18 March 2014
Accepted 23 March 2014
Available online 29 March 2014

Keywords:
Diesel emission control
Selective catalytic reduction (SCR)
NO_x reduction
Chabazite zeolite (CHA)
Reaction mechanism

ABSTRACT

In situ diffuse reflectance infrared Fourier transform spectroscopy (In situ DRIFTS), temperature-programmed desorption (TPD), and temperature-programmed surface reactions (TPSR) were employed to investigate the adsorption and reactive properties of Cu-SSZ-13 and Cu-SAPO-34 zeolite catalysts; these fully formulated washcoat cordierite monoliths were hydrothermally treated at 750 °C in the simulated feed gases. The intrinsic mechanism and reasons for the differences in NH_3-SCR activity were proposed based on the characterization results. The in situ DRIFTS and TPD results showed that ammonia could adsorb on both the Lewis and Brönsted acidic sites on these two catalysts; the ammonia on the Brönsted acidic sites might be active in the NH_3-SCR reaction. For the different NO_x adsorption processes, the total NO_x desorption levels followed the following sequence: $NO < NO + O_2 < NO_2 = NO_2 + O_2$. The results confirm that the reaction pathways are totally different in the low and high temperature ranges on the Cu-SSZ-13 and Cu-SAPO-34 catalysts. In the low temperature range, the ammonium nitrates from the reaction between surface ammonia and nitrates are the key intermediates and are further reduced to form N_2 and H_2O by the NO gas. In the high temperature range, the gas-phase NO_2 gradually become more important in the NH_3-SCR reaction. The activity tests indicated that the Cu-SAPO-34 catalyst had a relatively higher $DeNO_x$ performance than the Cu-SSZ-13 catalyst across the entire reaction temperature range, showing a double peak shapes with a dip point at approximately 390 °C. Cu-SAPO-34 might retain many surface nitrate species and did not produce much more NO_2 gas than Cu-SSZ-13; this species hindered the SCR reaction at 390 °C.

1. Introduction

Diesel engines offer numerous benefits, such as better fuel economy and lower CO_2 production, while emitting much higher levels of nitrogen oxides (NO_x); these species are the major cause of photochemical smog, acid rain, and ozone depletion. The selective catalytic reduction of NO_x with ammonia (NH_3-SCR) is one of the most effective methods to eliminate NO_x pollution [1]. Iron ion-exchanged zeolite catalysts perform well during the NH_3-SCR reaction used to control diesel emissions, and these compounds have been characterized in detail in recent decades [2–7]. However, copper ion-exchanged zeolite catalysts are much more active, selective, and hydrothermally stable for low temperature NH_3-SCR reactions (<350 °C) [8–12].

In recent years, copper zeolites with small pore structures, such as Cu-SSZ-13 and Cu-SAPO-34, have attracted attention for eliminating NO_x pollution. Both Cu-SSZ-13 and Cu-SAPO-34 show promising NO_x removal efficiency in NH_3-SCR reactions for the post-treatment systems on mobile sources [13–16]. Due to the potential applications of these catalysts, researchers have conducted extensive research, mainly focusing on the active copper species and their changes [17–30], the reaction intermediates [31], the acidity [32], the reaction mechanism [33–35], and the hydrothermal stability [36–38] of Cu-SSZ-13 and Cu-SAPO-34 in NH_3-SCR reactions. According to our recent results [37], the reaction mechanism may vary between the Cu-SSZ-13 and Cu-SAPO-34 catalysts due to their somewhat different reactivity. Currently, most studies of the reaction mechanism focus on Cu-SSZ-13, while some limited work has focused on Cu-SAPO-34. For Cu-SSZ-13, Szanyi and coworkers [31,35] found that nitrosyl species were easily bound to copper, indicating that the copper nitrosyl species were key intermediates during the NH_3-SCR reaction, especially at low

* Corresponding author. Tel.: +86 10 62771093.
E-mail address: lijunhua@tsinghua.edu.cn (J. Li).

http://dx.doi.org/10.1016/j.apcatb.2014.03.048
0926-3373/

temperatures. Later [33], they proposed that the ammonia species adsorbed on the copper ion sites were active and selective on the Cu-SSZ-13 catalyst at low temperatures, as further confirmed by a recent study [39]. Recently, Peden and coworkers [40] summarized the characterization and mechanistic studies in their review, explaining that both ammonia and NO_x could adsorb on the Cu ions of the Cu-CHA catalysts surface. Specially, the copper bonded nitrosyls were the critical intermediates [31] that reacted with H_2O and NH_3 to form NH_4NO_2 before decomposing into nitrogen and water at low temperatures. For Cu-SAPO-34, Epling and coworkers [34] found that the reaction between NO and NH_4NO_3 was the key step of the NH_3-SCR reaction. The reduction process could occur at 100 °C, enabling the low temperature SCR activity.

To our knowledge, few studies have compared Cu-SSZ-13 and Cu-SAPO-34 based on their activities and mechanisms. The aim of the present study is to gain insight into the differences of the NH_3-SCR performances and reaction mechanisms for commercial Cu-SSZ-13 and Cu-SAPO-34 catalysts using in situ diffuse reflectance infrared Fourier transform spectroscopy (In situ DRIFTS), temperature-programmed desorption (TPD), and temperature-programmed surface reaction (TPSR); these techniques can provide useful information regarding the adsorptive and reactive performance of gases on the catalyst surfaces [34,41–43]. In this study, Cu-SSZ-13 and Cu-SAPO-34 were purchased from two major catalyst producers and aged with water at 750 °C in the simulated gases. In situ DRIFTS was used to study the chemically adsorbed species, including different ammonia and nitrogen oxides, and their reactive properties during the transient reaction. Furthermore, to obtain the acidity and redox properties of the catalysts, TPD tests with NH_3 and NO_x (NO, NO + O_2, NO_2, NO_2 + O_2) were conducted at different adsorption temperatures. After the ammonia or NO_x gases were adsorbed on the catalyst surface, TPSR experiments were conducted: (1) NH_3 adsorbed species reacting with gaseous NO, NO_2, NO + O_2, NO_2 + O_2, NO + NO_2 or NO + NO_2 + O_2, (2) NO + O_2 adsorbed species reacting with gaseous NH_3 with or without O_2, and (3) NO_2 adsorbed species reacting with gaseous NH_3 with or without O_2.

2. Experimental

2.1. Catalysts

Cu-SSZ-13 and Cu-SAPO-34 zeolites are fully formulated washcoat cordierite monoliths taken from two major catalyst suppliers. These two catalysts were drilled into cores 1″ diameter × 1″ length. These cores obtained were aged individually at 750 °C for 16 h in a nitrogen gas mixture containing 14% O_2, 5% CO_2, and 5% H_2O; the cores were evaluated and characterized as described below. Finally, the washcoat catalysts were carefully scraped from the monolith cores and screened for further in situ DRIFTS studies. Because the catalytic activity and copper state of the Cu-zeolite might be affected by the copper contents [21,44,45], the copper loadings and other elemental compositions were determined in our previous study via inductively coupled plasma optical emission spectroscopy (ICP-OES) with an IRIS Intrepid II XSP apparatus from Thermo Fisher Scientific Inc. The results indicated that the copper contents were approximately 1.4 wt.% on Cu-SSZ-13 and 1.0 wt.% on Cu-SAPO-34, respectively [37]. In addition, the BET surface area of Cu-SSZ-13 and Cu-SAPO-34 catalysts were 266 and 289 m^2/g, respectively [37].

2.2. Catalyst activity tests

The catalytic activity was tested in a fixed-bed quartz tube reactor (1-inch internal diameter) containing the monolith cores (1″ diameter × 1″ length). The concentrations of NH_3, NO_x (NO, NO_2 and N_2O) and H_2O in the inlet and outlet gas were measured with an FTIR spectrometer from MKS Instruments, Inc. A N_2-based gas mixture containing 350 ppm NO, 350 ppm NH_3, 14% O_2, 5% CO_2, and 5% H_2O was introduced into the reactor, and the GHSV (gas hourly space velocity) was fixed at 60,000 or 80,000 h^{-1}. Note that, this GHSV is much higher than that used in our previous work [37]. Water vapor was generated by passing de-ionized water through heated band with a circulating pump. The catalytic activity was tested from 150 to 700 °C. To minimize the impact of the gas adsorption on the catalyst samples, the data were recorded after the reactions had achieved stable states.

2.3. In situ DRIFTS studies

The in situ diffuse reflectance infrared Fourier transform spectroscopy (DRIFTS) experiments were recorded with a Nicolet Nexus spectrometer equipped with a liquid nitrogen-cooled MCT detector. A Praying Mantis™ High Temperature Reaction Chamber from Harrick Scientific Products Inc. was used as the environmental chamber, while a dome with two KBr windows and one glass observation window were used on the chamber. Before the experiments, the samples were purged in flowing 10% O_2/N_2 at 500 °C for 60 min.

2.4. TPD and TPSR studies

The TPD and TPSR experiments were conducted using the same monolith catalyst as the activity test; this catalyst was treated with 10% O_2/N_2 at 600 °C for 60 min to remove any water and impurities adsorbed on its surface.

For the TPD experiments, the adsorption was performed by passing a mixed gas containing 500 ppm NH_3, 500 ppm NO, 500 ppm NO + 10% O_2, 500 ppm NO_2, or 500 ppm NO_2 + 10% O_2 with N_2 as the balance through a reaction bed at the desired temperature for 2 h. For NH_3-TPD, the adsorption process was carried out at 25 °C. For NO_x-TPD, adsorption process was conducted at 100 °C. The adsorption gas was purged with N_2 until no NH_3 or NO_x was detected in the effluent. The temperature-programmed measurements were performed up to 700 °C at 10 °C/min in the presence of N_2 flowing at 6.44 L/min.

TPSR tests for the reactions of the adsorbed ammonia with various gas-phase NO_x with or without O_2 were conducted. First, 500 ppm NH_3 was adsorbed at 100 °C. Subsequently, the sample was heated to 700 °C at 10 °C/min. Meanwhile, various gases (350 ppm NO, 350 ppm NO_2, 350 ppm NO + 10% O_2, 350 ppm NO_2 + 10% O_2, 350 ppm NO + 350 ppm NO_2, or 350 ppm NO + 350 ppm NO_2 + 10% O_2) were introduced. The reaction processes were named as follows: (1) $(NH_3)_{ad}$ + NO, (2) $(NH_3)_{ad}$ + NO_2, (3) $(NH_3)_{ad}$ + NO + O_2, (4) $(NH_3)_{ad}$ + NO_2 + O_2, (5) $(NH_3)_{ad}$ + NO + NO_2, and (6) $(NH_3)_{ad}$ + NO + NO_2 + O_2. In addition, the TPSR experiment for the reaction of the adsorbed NO_x with gas-phase NH_3 was also carried out: 500 ppm NO + 10% O_2 or 500 ppm NO_2 was first adsorbed at 100 °C. Subsequently, the sample was heated to 700 °C at 10 °C/min. Meanwhile, various gases (350 ppm NH_3 or 350 ppm NH_3 + 10% O_2) were introduced. The reaction processes were named as follows: (1) $(NO + O_2)_{ad}$ + NH_3, (2) $(NO + O_2)_{ad}$ + NH_3 + O_2, (3) $(NO_2)_{ad}$ + NH_3, and (4) $(NO_2)_{ad}$ + NH_3 + O_2. The constant total flow rate of the mixed gases was 6.44 L/min, and the concentrations of NH_3, NO, NO_2, and N_2O were continuously monitored with an FTIR spectrometer from MKS Instruments, Inc.

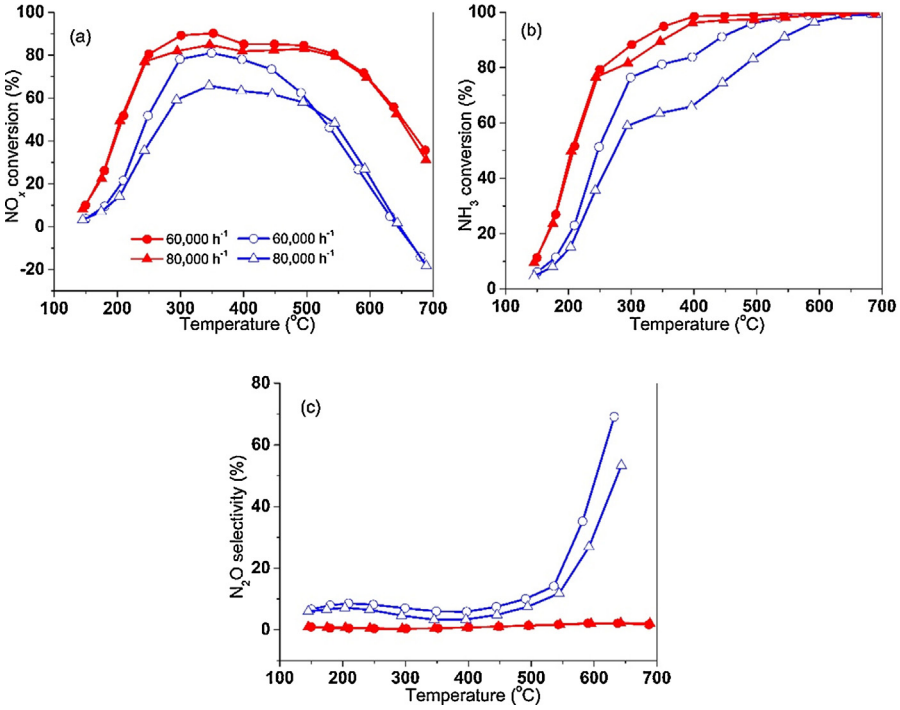

Fig. 1. Catalytic performance for SCR of NO_x with ammonia on Cu-SSZ-13 (blue) and Cu-SAPO-34 (red) monolith catalysts under different space velocity. Reaction conditions: 350 ppm NO, 350 ppm NH_3, 14% O_2, 5% CO_2, 5% H_2O, and N_2 as balance gas. (a) NO_x conversion on different catalysts; (b) NH_3 conversion on different catalysts; (c) N_2O selectivity on different catalysts. (For interpretation of the references to color in this figure legend, the reader is referred to the web version of the article.)

3. Results and discussion

3.1. SCR performance of different catalysts

Fig. 1(a) shows the $DeNO_x$ catalytic activity of the Cu-SSZ-13 and Cu-SAPO-34 monolith catalysts for the NH_3-SCR reaction at space velocities of 60,000 and 80,000 h^{-1}. At different space velocities, Cu-SAPO-34 showed relatively higher $DeNO_x$ activity than Cu-SSZ-13 across the entire temperature range. The catalytic activity of the Cu-SSZ-13 catalyst showed one volcano-shaped reaction curve. The maximum value of NO_x conversion (81%) was reached at 350 °C under space velocity of 60,000 h^{-1}; this value was 66% under high space velocity of 80,000 h^{-1}. The negative value for the NO_x conversions over Cu-SSZ-13 was ascribed to the strong ammonia oxidation above 650 °C. In addition, the NO_x conversions over Cu-SAPO-34 exceeded 80% in a wide temperature range (250–540 °C), decreasing to 55% at approximately 640 °C and continuing to decrease at increasing temperatures. The NO_x conversions over the Cu-SAPO-34 catalyst showed double peak shapes with a dip point at approximately 390 °C, peaking at approximately 350 and 500 °C, respectively. During the tests, the NO_x conversion data for these two catalysts were repeatable, and there was a dip point at approximately 390 °C for Cu-SAPO-34 [37]. Therefore, the differences in activity might indicate some mechanistic differences between these two catalysts, as discussed in the following section.

The NH_3 conversions for the NH_3-SCR reaction over Cu-SSZ-13 and Cu-SAPO-34 are summarized in Fig. 1(b). For the Cu-SAPO-34 catalyst, the NH_3 conversion values were almost identical to the NO_x conversion values below 300 °C, gradually increasing in the high temperature range and reaching nearly 100% above 400 °C. For Cu-SSZ-13, the NH_3 conversion was lower than for Cu-SAPO-34, was identical its own NO_x conversion values below 300 °C, and continued to increase above 350 °C. The above results indicate that NO_x reduction reaction occurred below 300 °C, while the NH_3 oxidation process gradually became dominant above 350 °C, decreasing the NO_x conversion slightly at high temperatures. Fig. 1(c) shows the N_2O selectivity for the NH_3-SCR reaction over these two catalysts. Cu-SSZ-13 yielded much more N_2O than Cu-SAPO-34, particularly above 500 °C.

N_2O usually comes from the decompositions of ammonium nitrates in NH_3-SCR reaction. However, this decomposition process mainly takes place at approximately 200 °C. For confirming the source of N_2O produced above 500 °C, the separate ammonia oxidation experiments were conducted using both Cu-SSZ-13 and Cu-SAPO-34 catalysts. Fig. 2 shows that NO was the main product in the ammonia oxidation reaction, while only small amounts of NO_2 (less than 10 ppm) were observed during the entire process. Due to the strong catalytic oxidation ability of ammonia at high temperatures, Cu-SSZ-13 selectively yielded much more NO and N_2O than Cu-SAPO-34 above 500 °C. These results implied that the source of N_2O produced above 500 °C primarily came from the ammonia oxidation process.

N_2O formation at high temperatures might be also related to the state of copper in Cu/zeolite catalysts. It was reported that the copper ion pairs, i.e. $[CuOCu]^{2+}$ dimers, were postulated as the active species for N_2O formation at high temperatures [46,47]. For both Cu-SSZ-13 and Cu-SAPO-34 catalysts, the distribution of copper species should be related with the copper concentrations [18,19] and hydrothermal treatment [36–38]. At high copper concentrations, copper ions mostly occupy in the large cages of the CHA structure rather than in the sites of the six-membered rings [18], and probably cause inferior N_2 selectivity in the SCR reaction [19]. Specially, these copper species in CHA sites agglomerate more readily due to less stable nature, leading to the formation of CuO_x [37,38]. According to our previous study [37], Cu-SSZ-13 was easily deactivated with the hydrothermal treatment, which might result from the formation of CuO_x aggregates or Cu dimers from migration of active copper sites. Therefore, the N_2 selectivity of Cu-SSZ-13 was reduced during the NH_3-SCR reaction at high temperatures.

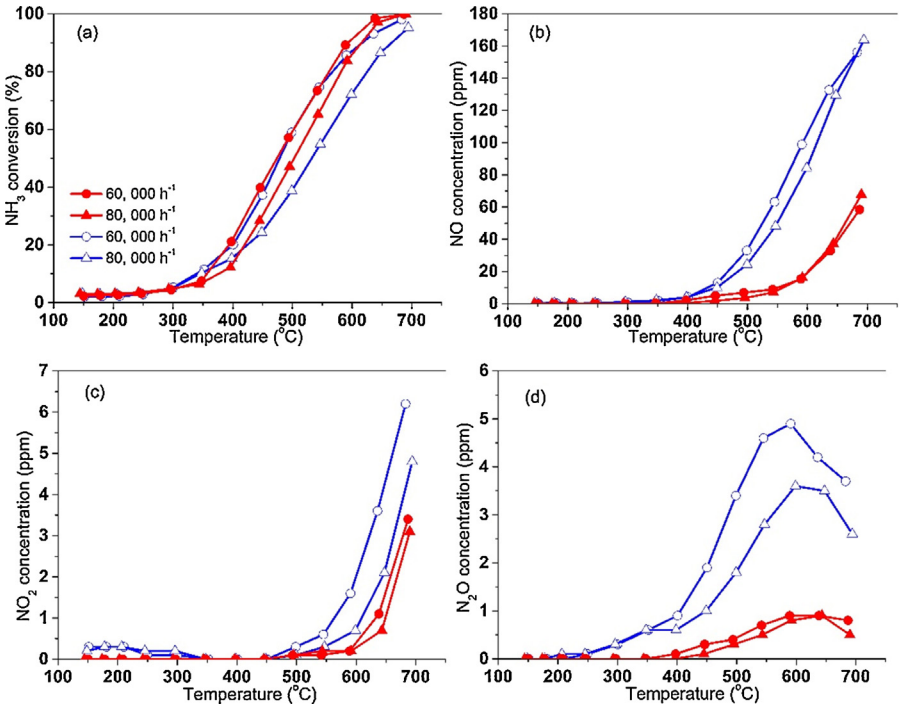

Fig. 2. Catalytic performance for ammonia oxidation on Cu-SSZ-13 (blue) and Cu-SAPO-34 (red) monolith catalysts under different space velocity. Reaction conditions: 350 ppm NH_3, 14% O_2, 5% CO_2, 5% H_2O, and N_2 as balance gas. (a) NH_3 conversion on different catalysts; (b) NO formation on different catalysts; (c) NO_2 formation on different catalysts; (d) N_2O formation on different catalysts. (For interpretation of the references to color in this figure legend, the reader is referred to the web version of the article.)

3.2. IR spectra of NH_3 adsorption and NH_3-TPD

The surface acid sites and their acidity can be determined using ammonia [48]. This information is obtained by studying the DRIFTS spectra of the adsorbed NH_3. The spectra of the adsorbed ammonia on the Cu-SSZ-13 and Cu-SAPO-34 at different temperatures are given in Fig. 3. For Cu-SSZ-13 catalysts, three strong bands at 3355, 3273, and 3181 cm^{-1} and four relatively weaker bands at 1617, 1493, 1449, and 1270 cm^{-1} were observed after the sample was treated in flowing 350 ppm NH_3/N_2 for 60 min and purged in N_2 at 25 °C. In the N–H stretching region, the bands at 3355 and 3273 cm^{-1} can be assigned to ammonium ions, while the band at 3181 cm^{-1} can be assigned to coordinated ammonia. The bands at 1493 and 1449 cm^{-1} are due to the bending vibration of NH_4^+ on the Brönsted acidic sites, while the bands at 1617 cm^{-1} and 1270 cm^{-1} can be assigned to bending vibrations of the N–H bonds in the NH_3 coordinated to the Lewis acidic sites (copper ion sites) [33,34,49,50]. The negative peaks at 3682 and 3600 cm^{-1} should be the O–H stretching bands of surface silanol and structural hydroxyl groups on Cu-SSZ-13, respectively [33]. The intensities of all the bands decreased when increasing the temperature indicating that the ammonia had desorbed. The IR bands of the coordinated NH_3 (1617 cm^{-1}) almost disappeared at 300 °C, while NH_4^+ ions (1449 cm^{-1}) were still detected at 400 °C in N_2. Therefore, the NH_4^+ ions on Brönsted acidic sites are much more stable at high temperatures than the ammonia adspecies on the Lewis acidic sites (copper ion sites). Compared to Cu-SSZ-13, similar features of ammonia adsorption were also observed during the adsorption process on Cu-SAPO-34. Several different adsorbed ammonia species appeared simultaneously: ammonium ions (3348 and 3276 cm^{-1}) and coordinated ammonia (3180 cm^{-1}) in the N–H stretching vibration region, and ammonium ions adsorbed on Brönsted (1495 and 1459 cm^{-1}) and Lewis acidic sites (copper ion sites) (1628 and 1266 cm^{-1}) in the N–H bending vibration region. Additionally, the ammonia adsorbed on Brönsted acid sites were much stronger than that on Lewis acid sites, and could

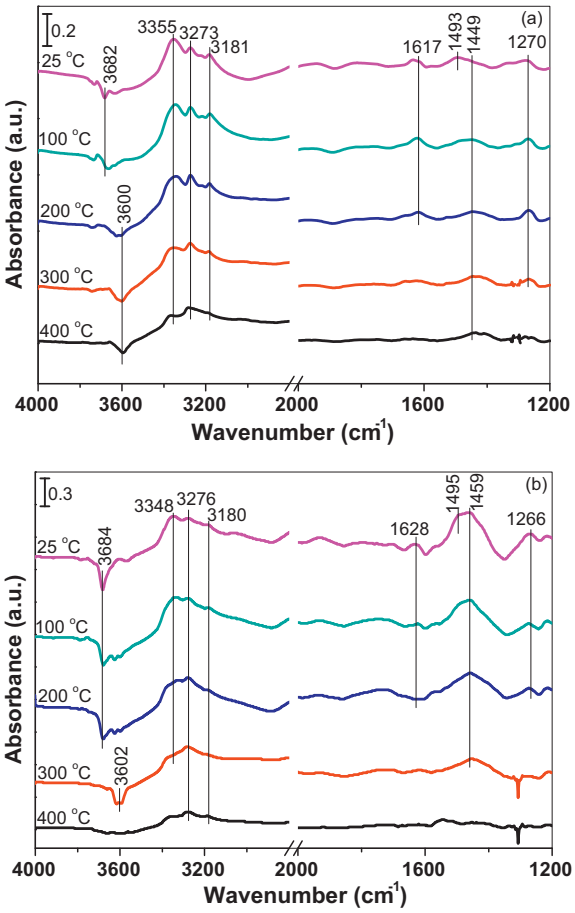

Fig. 3. DRIFTS spectra (100 scans) of chemisorbed 350 ppm NH_3/N_2 on (a) Cu-SSZ-13 and (b) Cu-SAPO-34 catalysts at 25 °C followed by purge in N_2 at different temperatures.

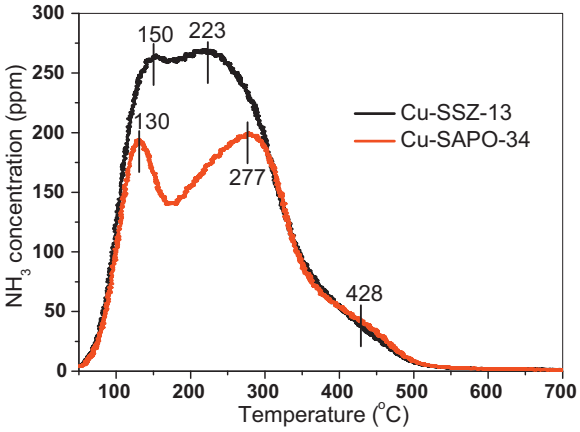

Fig. 4. NH_3-TPD profiles over Cu-SSZ-13 and Cu-SAPO-34 catalysts at room temperatures.

be still detected with the temperature rising above 300 °C. The above results suggested that the ammonia adsorption species on Cu-SAPO-34 should be similar to those on Cu-SSZ-13. Ammonia adsorbed on both the Lewis and Brönsted acidic sites for these two catalysts; the ammonia on the Lewis acidic sites was not as stable as that on the Brönsted acid sites, easily desorbing up to 300 °C.

Furthermore, the continuous adsorption of ammonia on Cu-SSZ-13 and Cu-SAPO-34 at different temperatures was also carried out. As shown in Figure S1, both coordinated NH_3 linked to the copper ion sites (the bands at 1268, 1617, and 3175 cm^{-1} for Cu-SSZ-13 and the bands at 1278, 1615, and 3166 cm^{-1} for Cu-SAPO-34) and ammonium ions adsorbed on the Brönsted acidic sites (the bands at 1424, 3270, and 3340 cm^{-1} for Cu-SSZ-13 and the bands at 1475, 3255, and 3340 cm^{-1} for Cu-SAPO-34) could be observed at 200 °C. Specially, the copper ion sites with bound ammonia remained stable up to 300 °C, nearly disappearing at 400 °C. Therefore, the ammonia adsorption species were similar to ammonia adsorption process in Fig. 3, confirming that ammonia might not significantly change copper species.

Fig. 4 shows the NH_3-TPD profiles for ammonia adsorption on the Cu-SSZ-13 and Cu-SAPO-34 at room temperature. For Cu-SSZ-13, a large peak including three main ammonia desorption peaks was observed over the entire desorption temperature range when the ammonia adsorption process was conducted at 25 °C. Two large ammonia desorption peaks were located at 150 and 223 °C, and a small peak was located at 428 °C. According to above IR results, the intensity of the ammonia on both the Lewis and Brönsted acidic sites slightly decreased between 100 and 200 °C; the intensity of the ammonia adsorption on Lewis acidic sites totally disappeared, while that on Brönsted acidic sites decreased between 200 and 300 °C. Furthermore, only the ammonia adsorbed on the Brönsted acidic sites was reduced above 300 °C. Therefore, the peak at 150 °C should be assigned to the physically adsorbed ammonia because these species generated a free NH_3 signal in the IR spectra. Meanwhile, the peak at 223 °C is assigned to ammonia adsorbed on the acid sites, including weakly and strongly bound NH_3 species (e.g. ammonia adsorbed on Lewis and Brönsted acidic sites); the peak at 428 °C is assigned to the ammonia strongly adsorbed on the Brönsted acidic sites [17,32,51]. For Cu-SAPO-34, there were three ammonia desorption peaks at 130, 277, and 428 °C observed across the entire temperature range, similar to the ammonia desorption trace for Cu-SSZ-13. These three peaks can also be ascribed to physically adsorbed ammonia species, ammonia adsorbed on acid sites including Lewis and Brönsted acidic sites, and ammonia adsorbed on strong Brönsted acidic sites, respectively. The

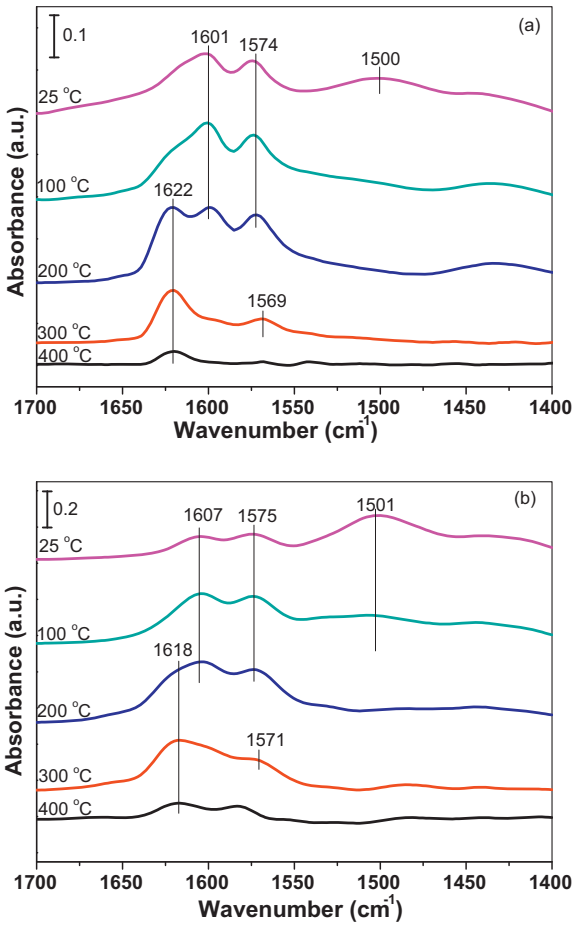

Fig. 5. DRIFTS spectra (100 scans) of chemisorbed 350 ppm NO + 10% O_2/N_2 on (a) Cu-SSZ-13 and (b) Cu-SAPO-34 catalysts at 25 °C followed by purge in N_2 at different temperatures.

temperature of the second peak for ammonia desorption on Cu-SAPO-34 was slightly higher than that on Cu-SSZ-13, implying Cu-SAPO-34 was more acidic. The NH_3-TPD experiments indicate that ammonia can be strongly adsorbed on the Cu-SSZ-13 and Cu-SAPO-34 catalysts. The total acid was calculated using the numerical integration of the totaled ammonia desorption peaks. The total amount of acid in Cu-SSZ-13 was higher than in Cu-SAPO-34 when the ammonia was adsorbed at 25 °C. However, the amount of ammonia desorption on these two catalysts was nearly identical above 200 °C (results not given). These results illustrate that the difference in acidity at low adsorption temperatures might be ascribed to the differences in the physical adsorbed ammonia related to the pore structure of these two catalysts [37], and there was no difference in total acidity at high adsorption temperatures.

3.3. IR spectra of NO_x adsorption and NO_x-TPD

To acquire information regarding different NO_x adsorbed species, the NO_x adsorption properties were also tested using in situ DRIFTS. In Fig. 5, the features in the IR spectra from approximately 1500–1650 cm^{-1} are formed over these two samples, and can be assigned to different nitrates and nitrites [49,52]. However, it is difficult to identify these peaks due to the very similar vibrations of the different nitrate species [34]. For example, Szanyi and coworkers [35] proposed that the bands near 1550–1630 cm^{-1} for Cu-SSZ-13 were attributed to nitrate species. Iwasaki and

coworkers [53] thought that the bands at 1656 (and 1635) and 1590 (and 1572) cm^{-1} were assigned to the nitro and nitrate groups, respectively. Yang and coworkers [54] thought that the bands at 1622 and 1568 cm^{-1} were attributed to adsorbed NO_2 and nitrate species, respectively. Consequently, we speculated that the three IR bands could be attributed to monodentate nitrates (1601 cm^{-1} for Cu-SSZ-13 and 1607 cm^{-1} for Cu-SAPO-34) [34,52], bidentate nitrates (1574 cm^{-1} for Cu-SSZ-13 and 1575 cm^{-1} for Cu-SAPO-34) [34,52], nitrites (1500 cm^{-1} for Cu-SSZ-13 and 1501 cm^{-1} for Cu-SAPO-34) adspecies [52], respectively. The nitrites were assigned based on two reasons. First, the IR bands at approximately 1500 cm^{-1} was not stable at high temperatures and would easily desorb/decompose above 100 °C. Second, in the NO_x-TPD results, a small amount of NO was the main desorption products for the NO_x desorption peaks at approximately 140 °C, while a large amount of NO_2 was the main desorption product at high temperature ranges. Therefore, the adsorbed nitrate and nitrite species might generate different desorption products: NO_2 and NO in the gas-phase. As shown in Fig. 5, the nitrite species quickly disappeared when the temperature increased above 100 °C. As the temperature increased to 200 °C, the bidentate and monodentate nitrates sharply decreased, while a new intense band at 1622 cm^{-1} and 1618 cm^{-1} formed for Cu-SSZ-13 and Cu-SAPO-34, revealing the formation of surface adsorbed NO_2 [54]. Further increasing the temperature to 300 °C generated a new band at 1569 cm^{-1} for Cu-SSZ-13 and 1571 cm^{-1} for Cu-SAPO-34, implying the formation of nitrate species at high temperatures. At high temperatures, rapid NO oxidation and NO_2 dissociation would take place, forming additional stable nitrates.

Various NO_x-TPD experiments are conducted on Cu-SSZ-13 and Cu-SAPO-34 catalysts and are summarized in Fig. 6. For the $NO_2 + O_2$ adsorption onto Cu-SSZ-13, only one small peak at 140 °C and three groups of NO_x desorption peaks at 240, 330, and 384 °C were apparent. As mentioned above, the peaks at 140 °C might be ascribed to surface nitrite decomposition, while the peaks at high temperatures indicated the decomposition of monodentate, chelating and bridging bidentate nitrates on the Cu-SSZ-13 catalyst, respectively. There were almost no differences between the shapes of the NO_x desorption curves when $NO_2 + O_2$ and NO_2 were adsorbed onto Cu-SSZ-13. Compared to $NO_2 + O_2$ or NO_2, the NO_x desorption peaks were obviously inhibited during the $NO + O_2$ adsorption process, and the desorption peaks were only observed at 330 and 384 °C. Furthermore, only a small amount of NO_x desorption was observed for the NO adsorption process. Four different NO_x desorption curves illustrate that O_2 is critical during NO_x adsorption, facilitating NO oxidation and the formation of nitrate species on the surface that later decompose to form NO_x (mainly NO_2) gas. In addition, similar to Cu-SSZ-13, one weak NO_x desorption peak was apparent at 150 °C, while two strong NO_x desorption peaks were observed at 290 and 387 °C on Cu-SAPO-34 for the $NO_2 + O_2$ or NO_2 adsorption process. These three peaks can be attributed to the decomposition of surface nitrite, chelating, and bridging bidentate nitrates, respectively. Specially, the desorption intensity of the chelating bidentate nitrates at 290 °C was similar to that of Cu-SSZ-13, but the intensity of bridging bidentate nitrates at 387 °C was much stronger than Cu-SSZ-13. Therefore, NO_x can be easily transformed into various stable species, including bridging bidentate nitrates, formed on Cu-SAPO-34 catalyst surface, generating more NO_2 in the gas phase. In addition, for the $NO + O_2$ or NO adsorption process on Cu-SAPO-34, only one strong peak at 395 °C was observed in the high temperature range aside from the nitrite decomposition at 150 °C; the latter represented the formation of bridging bidentate nitrates.

During these NO_x-TPD tests, NO, $NO + O_2$, NO_2, and $NO_2 + O_2$ were selected to test the differences in NO_x adsorption abilities of Cu-SSZ-13 and Cu-SAPO-34. For both catalysts, NO_2 was the main species desorbed above 200 °C based on the NO_x-TPD experiments. The total NO_x desorption levels are as follows: $NO < NO + O_2 < NO_2 = NO_2 + O_2$. This result is consistent with the DRIFTS study of NO, $NO + O_2$, and NO_2 adsorption on Cu-SAPO-34 catalyst [34]: the nitrate concentrations formed on the surface follow the same order as our study. Moreover, large differences in the NO_x adsorbed species were apparent between the $NO + O_2$ and NO_2 adsorption processes. The NO_2 adsorption process produced more surface nitrate species than the $NO + O_2$ adsorption process, indicating that the NO_2 adsorption process was a fast reaction and that the NO oxidation process was much slower.

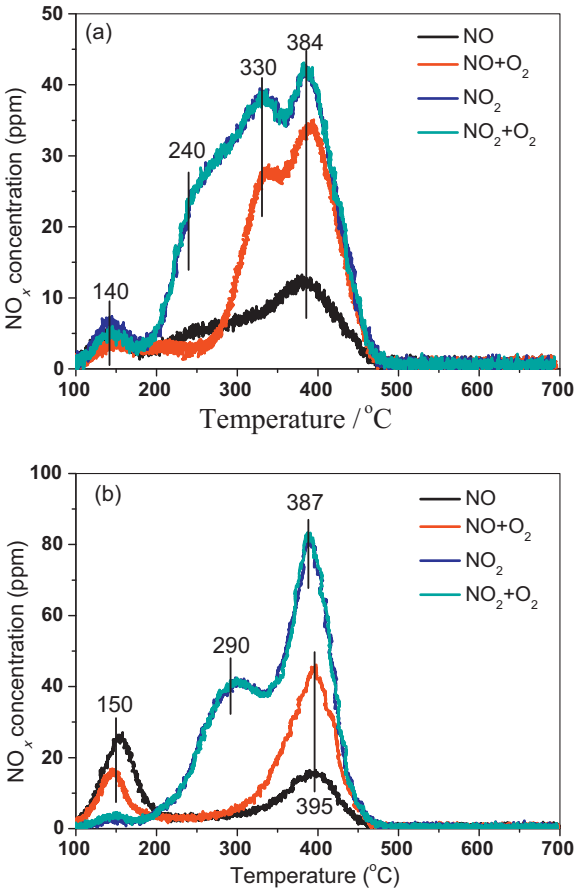

Fig. 6. NO_x-TPD profiles of different NO_x adsorption with or without oxygen over (a) Cu-SSZ-13 and (b) Cu-SAPO-34 catalysts at 100 °C.

The process of NO oxidation to NO_2, subsequently forming the surface nitrates, is crucial during the NH_3-SCR reaction [54–56]. Therefore, during NO_x adsorption process, NO was slowly oxidized to NO_2 before quickly forming a heterogeneous nitrate species on Cu-SSZ-13 and Cu-SAPO-34. In the NO_x-TPD experiments, the major difference between Cu-SSZ-13 and Cu-SAPO-34 is the NO_x desorption intensity at approximately 390 °C (Fig. 6). This behavior might be related to the oxidation or chemical adsorption abilities for nitrates on these two catalysts. On Cu-SAPO-34, many additional stable nitrate species, including the bridging bidentate nitrates, would be formed and would be adsorbed. The additional formation should be related to the different oxidative abilities of these two catalysts. A comparison of the oxidative activity from NO to NO_2 in the presence of O_2 on Cu-SSZ-13 and Cu-SAPO-34 catalysts is shown in Figure S2. Obviously, Cu-SAPO-34 has a stronger oxidative ability than Cu-SSZ-13. The oxidation rate from NO to NO_2 increased with the temperature, reaching a maximum conversion of 49.2% on Cu-SAPO-34

and 35.4% on Cu-SSZ-13 at 400 °C before decreasing from 400 to 650 °C.

3.4. Reactivity of the ammonia adspecies and nitrogen oxides

The NH_3-SCR reaction mechanism was studied extensively on copper or iron ion-exchanged zeolites; the mechanism might change with the temperature [33,34,40,54,55,57,58]. Considering catalytic performance of NH_3-SCR on both Cu-SSZ-13 and Cu-SAPO-34, the in situ DRIFTS experiments for the transient reaction were conducted at 220 °C and 350 °C, respectively. In addition, the features of the ammonia species in both the high and low wavenumber regions would change in parallel during the ammonia adsorption and reaction processes [33]. Accordingly, the following will focus on the adsorbed ammonia spectral change in the N–H bending vibration region, particularly for ammonia adsorbed on the Brönsted (bands at approximately 1445 cm^{-1}) and Lewis acidic sites (bands at approximately 1617 cm^{-1}).

The IR spectra of the reaction between the adsorbed ammonia species and NO, NO + O_2, NO_2, or NO + NO_2 at 220 °C are shown in Figures S3, S4, S5, and S6. After different NO_x mixtures were passed over the surface of the ammonia-adsorbed Cu-SSZ-13 and Cu-SAPO-34, the intensity of Brönsted acid bound NH_4^+ significantly decreased. Meanwhile, some new bands at approximately 1570–1620 cm^{-1} would appear, particularly on the Cu-SAPO-34 catalysts, indicating the formation of nitrate species and NO_2 during this process. In these results, the Lewis acidic sites coordinated with ammonia did not change obviously during the transient reaction. There are two reasons for this phenomenon. First, the ammonia adsorbed on the Lewis acidic sites might not be very active for the SCR reaction in these tests. Second, the peaks for the Lewis acid bound ammonia might be obscured by the broad IR bands for the nitrate/NO_2 formation.

In the transient reaction, the integrated area of the bands at approximately 1445 cm^{-1} represent the reaction between the adsorbed NH_4^+ and NO, NO + O_2, NO_2, or NO + NO_2 on Cu-SSZ-13 and Cu-SAPO-34; these areas are calculated and summarized in Fig. 7. As shown in Fig. 7(a), for Cu-SSZ-13, the IR band attributed to the NH_4^+ ions decreased to 24% of the initial intensity after NO was passed over the catalyst surface for 15 min. When both NO and O_2 were passed over the catalyst surface, the catalytic reaction was slightly improved, reaching 18% of the initial intensity after 15 min. However, the catalytic reaction was greatly improved when NO and NO_2 were simultaneously passed over the samples; the signal for the NH_4^+ ions gradually decreased after 7 min and diminished within 12 min. However, during the process between adsorbed NH_4^+ and gas-phase NO_2, the signal for the NH_4^+ ions remained stable, merely decreasing to 72% of the initial intensity after 15 min. The present results demonstrate that at low temperatures the presence of oxygen increased the reaction rate between the adsorbed NH_4^+ ions and the gas-phase NO_x. However, the presence of NO_2 should not be critical for this reaction process. Fig. 7(b) shows that for Cu-SAPO-34, the NH_4^+ ions were almost completely consumed within 2 min for NO + NO_2, 3 min for NO + O_2, 4 min for NO, and 10 min for NO_2, respectively. Therefore, the reaction rate for Cu-SAPO-34 was significantly improved compared to Cu-SSZ-13. Moreover, similar to Cu-SSZ-13, the reactivity of the NH_4^+ ions on Cu-SAPO-34 decreased in the following sequence: NO + NO_2 > NO + O_2 > NO > NO_2. The sequence of the reaction rates between the adsorbed NH_4^+ and the different NO_x should be similar on Cu-SSZ-13 and Cu-SAPO-34. Therefore, at low temperatures, the NH_3-SCR reaction might follow the same routes over both catalysts.

Furthermore, similar transient reaction tests at high temperatures were also conducted. The IR spectra of the reaction between the adsorbed ammonia and NO, NO + O_2, or NO_2 at 350 °C are given in Figures S7, S8, and S9, respectively. The IR bands for the ammonia coordinated to the Lewis acidic sites were very weak, while the NH_4^+ adsorbed on the Brönsted acidic sites generated a much more intense peak that changed gradually during the reaction. Similarly, the bands at approximately 1445 cm^{-1} were calculated and summarized in Fig. 8. Therefore, on both Cu-SSZ-13 and Cu-SAPO-34, the reactivity with NH_4^+ ions decreased in the following sequence: NO_2 > NO + O_2 > NO. For Cu-SSZ-13, the fastest response between the NH_4^+ ions and the gas-phase NO_2 occurred over 8 min, while the NH_4^+ ions on Cu-SAPO-3 were totally consumed within 2 min for NO_2, 4 min for NO + O_2, and 7 min for NO process, respectively. These results are consistent with the catalytic performance of these two materials, further demonstrating that the NH_3-SCR reaction rate on Cu-SAPO-34 is much faster than on Cu-SSZ-13.

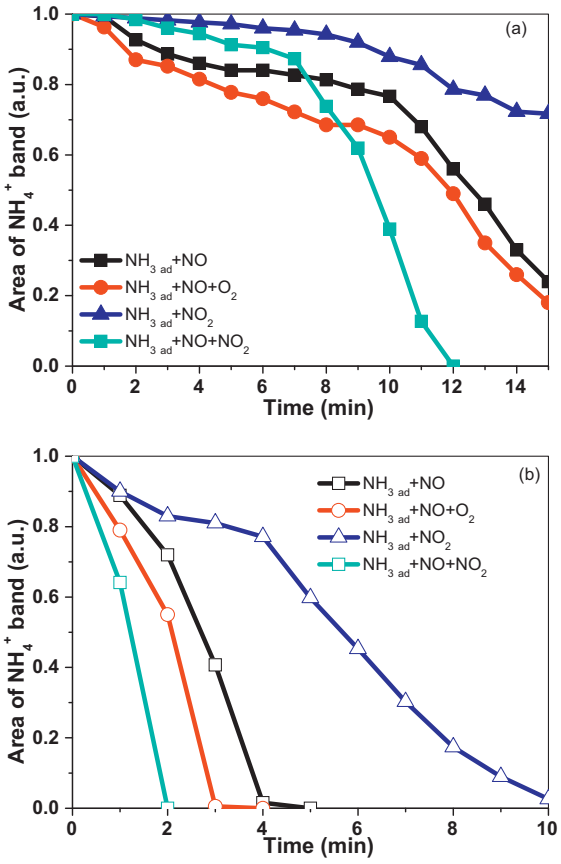

Fig. 7. Consumption of NH_4^+ ions (indicated by normalized band area at approximately 1445 cm^{-1}) at 220 °C upon passing 350 ppm NO/N_2, 350 ppm NO + 10% O_2/N_2, 350 ppm NO_2/N_2, and 175 ppm NO + 175 ppm NO_2/N_2 over (a) Cu-SSZ-13 and (b) Cu-SAPO-34 catalysts with preadsorbed NH_3.

Figures S10 and S11 show the TPSR results for the reaction between the adsorbed ammonia and the gas-phase NO, NO_2, NO + O_2, NO_2 + O_2, NO + NO_2, or NO + NO_2 + O_2 over Cu-SSZ-13 and Cu-SAPO-34. The NH_3-SCR reaction rate was increased after adding oxygen (based on the reaction between the adsorbed NH_3 and the gas-phase NO or NO + O_2). However, few differences were apparent in the reaction between $(NH_3)_{ad}$ + NO_2 and $(NH_3)_{ad}$ + NO_2 + O_2. Therefore, oxygen primarily promoted the NO oxidation to form NO_2 on Cu-SSZ-13 and Cu-SAPO-34. Moreover, after adding NO_2 to the reaction, a large amount of N_2O formed from 150 to 340 °C (based on the $(NH_3)_{ad}$ + NO_2 and $(NH_3)_{ad}$ + NO_2 + O_2 reactions). These results indicate that nitrates would quickly build up in the presence of NO_2, forming additional ammonium nitrates and decomposing into N_2O across a higher temperature range (approximately 200 °C). In addition, when NO + NO_2 or NO + NO_2 + O_2

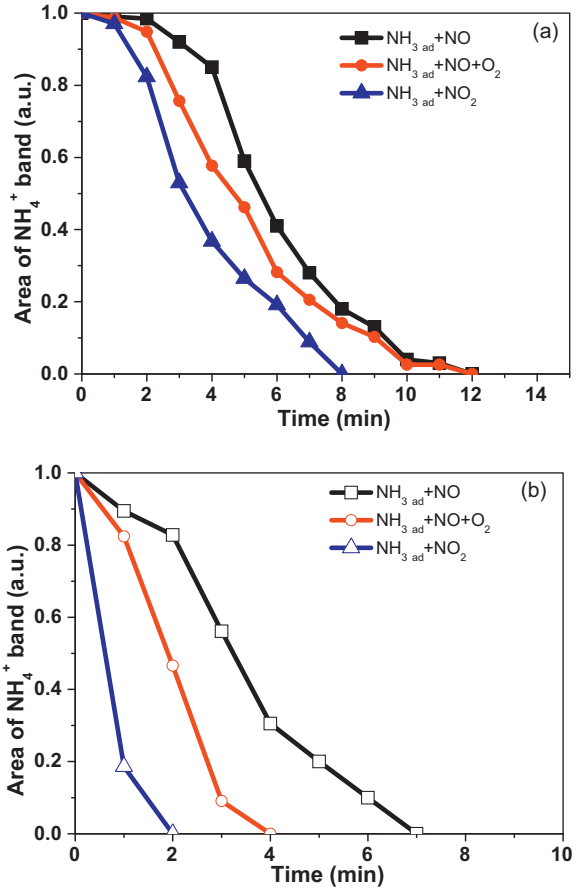

Fig. 8. Consumption of NH_4^+ ions (indicated by normalized band area at approximately 1445 cm^{-1}) at 350 °C upon passing 350 ppm NO/N_2, 350 ppm NO + 10% O_2/N_2, and 350 ppm NO_2/N_2 over (a) Cu-SSZ-13 and (b) Cu-SAPO-34 catalysts with preadsorbed NH_3.

were introduced into the reaction, almost no NH_3 desorption was observed during the TPSR tests, indicating that a "fast SCR" reaction occurred. The adsorbed ammonia would be consumed by the reaction with NO + NO_2 or NO + NO_2 + O_2 in the "fast SCR" reaction path [34].

3.5. Reactivity of the nitrogen oxide adspecies and ammonia

To identify the reactive NO_x species on the catalyst surface and study the reaction pathways at high temperatures, TPSR experiments were conducted by saturating Cu-SSZ-13 or Cu-SAPO-34 monolith catalysts with NO_x species, followed by heating in flowing ammonia with or without oxygen. Little NO_x desorption was observed near 130 °C for these two catalysts, and no other NO_x desorption was observed across the entire temperature range. Therefore, the NO_x signal is not provided in these results. Figure S12 shows that the ammonia signal increased up to 235 °C over Cu-SSZ-13, sharply decreasing its minimum value (approximately 290 °C) before increasing again at higher temperatures. The ammonia signal decreased steeply at approximately 290 °C for the pre-adsorption of NO_2 than for the pre-adsorption of NO + O_2. Therefore, ammonia reacted with the adsorbed NO_x species between 235 and 290 °C and was not consumed further due to the lower residual nitrate species content on the catalyst surface. For the NO + O_2 or NO_2 preadsorption process, the ammonia signal continued to decrease at temperatures above 235 °C when NH_3 + O_2 were introduced simultaneously. Therefore, the ammonia oxidation reaction primarily occurred in the presence of oxygen at high temperature. The TPSR trace for Cu-SAPO-34 catalyst was similar to that of Cu-SSZ-13. The ammonia signal decreased at temperatures above 230 °C, before decreasing to a concave point at approximately 300 °C and increasing again. The preadsorbed NO_2 consumes much more ammonia than the preadsorbed NO + O_2 species, remaining consistent with that of Cu-SSZ-13, indicating that NO_2 can generate much higher levels of nitrate species on the catalyst surface.

3.6. Possible reaction pathways

In this study, the TPSR ammonia traces (Figure S12) had a clear relationship with the NO_x desorption traces on Cu-SSZ-13 and Cu-SAPO-34 during NO_x-TPD (Fig. 6). A broad NO_x desorption peak (mainly NO_2 desorption) was observed between 250 and 450 °C during the NO_x-TPD experiments; ammonia was consumed within this exact temperature range during the TPSR experiments. Therefore, the adsorbed ammonia reacted with the gas-phase NO_2, validating the transient DRIFTS results (Fig. 8). Therefore, the NH_3-SCR reaction mechanism at high temperatures for Cu-SSZ-13 and Cu-SAPO-34 should comply with the following path. Ammonia was first adsorbed at the zeolitic acid sites. Afterward, NO was oxidized to form NO_2 on the Cu-zeolite surface at high temperatures. The gas-phase NO_2 might be an important intermediate during the NH_3-SCR reaction. The preadsorbed ammonia would react with the gas-phase NO_2 to form intermediates before decomposing to form N_2 and H_2O. Due to its facile adsorption of surface nitrate species (Fig. 6), Cu-SAPO-34 does not yield as much gas-phase NO_2 as Cu-SSZ-13. The SCR activity trace for Cu-SAPO-34 displays a dip at approximately 390 °C.

Increasingly, NO oxidation is reported as a fast process on Cu-SSZ-13 and Cu-SAPO-34, particularly at high copper loadings (Figure S2) [19]. Therefore, this traditionally termed "standard SCR" process might be a "fast SCR" process on these two catalysts. As shown in Figure S13, the presence of NO + NO_2 improves the NO_x conversions for the NH_3-SCR reaction at low temperatures, remaining consistent with the transient DRIFTS results (Fig. 7). In addition, both Cu-SSZ-13 and Cu-SAPO-34 had an excellent N_2 selectivity at low temperatures (Fig. 1(c)), implying that the formation of NH_4NO_3 would be quickly decreased and demonstrating that only portions of the NO were oxidized into NO_2 and that the remaining NO would reduce adsorbed ammonium nitrates to form nitrogen and water during the NH_3-SCR reaction.

Furthermore, DRIFTS study was carried out to confirm the key intermediates formed on Cu-SSZ-13 and Cu-SAPO-34 catalysts at low temperatures. After exposure to NH_3 and NO_2 at 220 °C for 30 min, the catalysts were purged in the presence of N_2 for another 20 min, and then NO/N_2 were introduced into the gas chamber, while the IR signals were recorded with time passing. As shown in Fig. 9, the bands at 1598 and 1568 cm^{-1} for Cu-SSZ-13 and the bands at 1598 and 1571 cm^{-1} for Cu-SAPO-34 appeared, which were consistent with the IR signals, located at 1596 and 1575 cm^{-1}, generated from pure NH_4NO_3 powder on Cu-SAPO-34 [34]. It is evident that the ammonium nitrates would be formed on both Cu-SSZ-13 and Cu-SAPO-34 catalysts. With NO introducing into the reaction chamber, the ammonium nitrate signals significantly changed and almost completely disappeared after 20 min for Cu-SSZ-13 and 10 min for Cu-SAPO-34. Meanwhile, the new bands at 1627 cm^{-1} or 1621 cm^{-1} appeared, being indicative of NO_2 adsorbed species [54]. The above results further proves that the surface intermediates, ammonium nitrates, would be active with gas-phase NO. The NH_3-SCR reaction path at low temperatures resembles the mechanism: ammonium nitrates from the reaction between the surface ammonia and the nitrates are the key intermediates and are further reduced to form N_2 and H_2O by gas-phase NO.

It is well recognized that NH_3-SCR performance on Cu-SSZ-13 and Cu-SAPO-34 catalysts should be mainly ascribed to zeolite

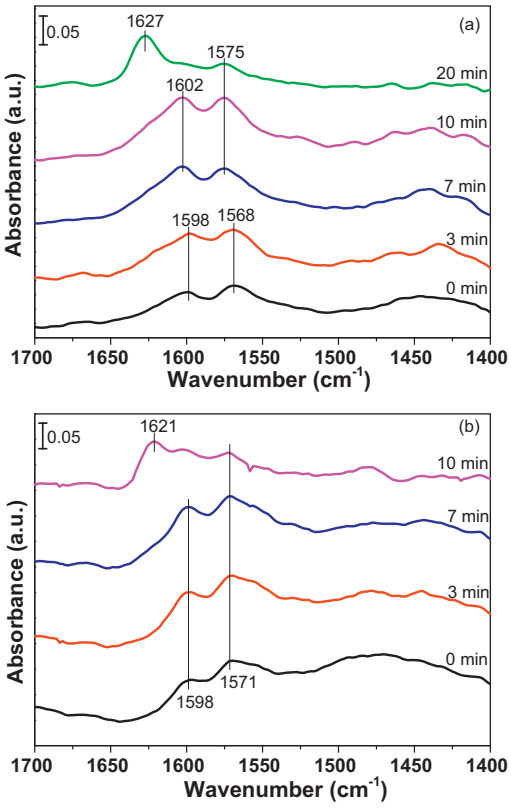

Fig. 9. DRIFTS spectra (100 scans) taken at 220 °C upon passing 350 ppm NO/N_2 over (a) Cu-SSZ-13 and (b) Cu-SAPO-34 catalysts with preadsorbed NH_3 and NO_2.

acidity and copper sites. The acidic sites of chabazite zeolite supports contributed to the ammonia adsorption or activation, while the copper sites were responsible for the NO_x activation or oxidation. To deeply understand the critical factor for determining the catalytic activity, these two kinds of sites should be considered and discussed. As discussed in NH_3-TPD section, there was no difference in total acidity at the adsorption temperatures above 200 °C between these two catalysts, and the differences in the physical adsorbed ammonia was mainly related to the pore structure. Furthermore, the activity tests implied that Cu-SAPO-34 commercial monolith catalyst was more active and selective for N_2 production than Cu-SSZ-13 catalyst for NH_3-SCR under high space velocity, especially in the medium/high temperature ranges. Considering the excellent NH_3-SCR performance mainly taking place above 200 °C, we speculated that the acidic sites might not be the critical factors for SCR reaction. In addition, in recent years, more and more research results demonstrated that the isolated Cu^{2+} species was the active sites for NH_3-SCR reaction for Cu-SSZ-13 and Cu-SAPO-34 [17,20,21,28–30]. As discussed in this study, the reaction mechanism should follow different ways with the temperature changing. Therefore, the active copper species should be responsible for NO activation and oxidation for the formation of nitrates in low temperatures and formation of NO_2 in high temperatures. It seems that Cu-SSZ-13 was much easier to be deactivated with the hydrothermal treatment [37]. The formation of CuO_x aggregates or Cu dimers from migration of active copper sites [37], i.e. isolated Cu^{2+} species, was supposed to contribute the reduced NH_3-SCR activity and N_2O formation [22].

4. Conclusions

Cu-SSZ-13 and Cu-SAPO-34 from two major catalyst suppliers were tested in NH_3-SCR reactions. Cu-SAPO-34 showed higher $DeNO_x$ catalytic activity than did the Cu-SSZ-13 catalyst across the entire temperature range while showing double peak shapes with a dip point at approximately 390 °C, thereby revealing mechanistic differences between these two catalysts. Ammonia could adsorb on both the Lewis and Brönsted acidic sites for these two catalysts, while the ammonia on the Brönsted acid sites was active in the NH_3-SCR reaction. For different NO_x adsorption processes, the total NO_x desorption levels occurred in the following sequence: $NO < NO + O_2 < NO_2 = NO_2 + O_2$. The reaction pathways are completely different in the low and high temperature ranges for both Cu-SSZ-13 and Cu-SAPO-34. In the low temperature range, the ammonium nitrates from the reaction between surface ammonia and nitrates are the key intermediates that are further reduced by gas-phase NO to form N_2 and H_2O. In the high temperature range, the gas-phase NO_2 is an important intermediate in the NH_3-SCR reaction. The preadsorbed ammonia will react with gas-phase NO_2 to form the intermediate before decomposing to form the final products: N_2 and H_2O. Cu-SAPO-34 might retain numerous surface nitrate species and did not produce notably more gas-phase NO_2 than Cu-SSZ-13, hindering the SCR reaction at 390 °C.

Acknowledgements

This work was financially supported by National Natural Science Foundation of China (21325731) and National High-Tech Research and Development (863) Program of China (2013AA065304). Lei Ma gratefully acknowledges the financial support provided by special fund of State Key Joint Laboratory of Environment Simulation and Pollution Control (13K04ESPCT) and China Postdoctoral Science Foundation (2013M530643).

Appendix A. Supplementary data

Supplementary data associated with this article can be found, in the online version, at http://dx.doi.org/10.1016/j.apcatb.2014.03.048.

References

[1] P. Granger, V.I. Parvulescu, Chem. Rev. 111 (2011) 3155–3207.
[2] R.Q. Long, R.T. Yang, J. Am. Chem. Soc. 121 (1999) 5595–5596.
[3] T.J. Wang, S.W. Baek, H.J. Kwon, Y.J. Kim, I.-S. Nam, M.-S. Cha, G.K. Yeo, Ind. Eng. Chem. Res. 50 (2011) 2850–2864.
[4] Y.J. Kim, H.J. Kwon, I. Heo, I.-S. Nam, B.K. Cho, J.W. Choung, M.-S. Cha, G.K. Yeo, Appl. Catal. B: Environ. 126 (2012) 9–21.
[5] L. Ma, H. Chang, S. Yang, L. Chen, L. Fu, J. Li, Chem. Eng. J. 209 (2012) 652–660.
[6] L. Ma, J. Li, H. Arandiyan, W. Shi, C. Liu, L. Fu, Catal. Today 184 (2012) 145–152.
[7] L. Ma, J. Li, Y. Cheng, C.K. Lambert, L. Fu, Environ. Sci. Technol. 46 (2012) 1747–1754.
[8] J. Baik, S. Yim, I.-S. Nam, Y. Mok, J.-H. Lee, B. Cho, S. Oh, Top. Catal. 30-31 (2004) 37–41.
[9] A. Sultana, T. Nanba, M. Haneda, M. Sasaki, H. Hamada, Appl. Catal. B-Environ. 101 (2010) 61–67.
[10] S.S.R. Putluru, A. Riisager, R. Fehrmann, Appl. Catal. B-Environ. 101 (2011) 183–188.
[11] S. Andonova, E. Vovk, J. Sjöblom, E. Ozensoy, L. Olsson, Appl. Catal. B: Environ. 147 (2014) 251–263.
[12] B. Pereda-Ayo, U. De La Torre, M.J. Illán-Gómez, A. Bueno-López, J.R. González-Velasco, Appl. Catal. B: Environ. 147 (2014) 420–428.
[13] J.H. Kwak, R.G. Tonkyn, D.H. Kim, J. Szanyi, C.H.F. Peden, J. Catal. 275 (2010) 187–190.
[14] D.W. Fickel, E. D'Addio, J.A. Lauterbach, R.F. Lobo, Appl. Catal. B-Environ. 102 (2011) 441–448.
[15] R. Martínez-Franco, M. Moliner, C. Franch, A. Kustov, A. Corma, Appl. Catal. B: Environ. 127 (2012) 273–280.
[16] L. Xie, F. Liu, L. Ren, X. Shi, F.-S. Xiao, H. He, Environ. Sci. Technol. 48 (2013) 566–572.
[17] L. Wang, W. Li, G. Qi, D. Weng, J. Catal. 289 (2012) 21–29.
[18] J.H. Kwak, H.Y. Zhu, J.H. Lee, C.H.F. Peden, J. Szanyi, Chem. Commun. 48 (2012) 4758–4760.
[19] J. Kwak, D. Tran, J. Szanyi, C. Peden, J. Lee, Catal. Lett. 142 (2012) 295–301.
[20] S.T. Korhonen, D.W. Fickel, R.F. Lobo, B.M. Weckhuysen, A.M. Beale, Chem. Commun. 47 (2011) 800–802.
[21] J. Xue, X. Wang, G. Qi, J. Wang, M. Shen, W. Li, J. Catal. 297 (2013) 56–64.

[22] U. Deka, I. Lezcano-Gonzalez, S.J. Warrender, A. Lorena Picone, P.A. Wright, B.M. Weckhuysen, A.M. Beale, Microporous Mesoporous Mater. 166 (2013) 144–152.
[23] P.N.R. Vennestrøm, A. Katerinopoulou, R.R. Tiruvalam, A. Kustov, P.G. Moses, P. Concepcion, A. Corma, ACS Catal. 3 (2013) 2158–2161.
[24] F. Göltl, R.E. Bulo, J. Hafner, P. Sautet, J. Phys. Chem. Lett. 4 (2013) 2244–2249.
[25] F. Giordanino, P.N.R. Vennestrom, L.F. Lundegaard, F.N. Stappen, S. Mossin, P. Beato, S. Bordiga, C. Lamberti, Dalton Trans. 42 (2013) 12741–12761.
[26] S. Fan, J. Xue, T. Yu, D. Fan, T. Hao, M. Shen, W. Li, Catal. Sci. Technol. 3 (2013) 2357–2364.
[27] J.S. McEwen, T. Anggara, W.F. Schneider, V.F. Kispersky, J.T. Miller, W.N. Delgass, F.H. Ribeiro, Catal. Today 184 (2012) 129–144.
[28] U. Deka, A. Juhin, E.A. Eilertsen, H. Emerich, M.A. Green, S.T. Korhonen, B.M. Weckhuysen, A.M. Beale, J. Phys. Chem. C 116 (2012) 4809–4818.
[29] S.A. Bates, A.A. Verma, C. Paolucci, A.A. Parekh, T. Anggara, A. Yezerets, W.F. Schneider, J.T. Miller, W.N. Delgass, F.H. Ribeiro, J. Catal. 312 (2014) 87–97.
[30] U. Deka, I. Lezcano-Gonzalez, B.M. Weckhuysen, A.M. Beale, ACS Catal. 3 (2013) 413–427.
[31] J.H. Kwak, J.H. Lee, S.D. Burton, A.S. Lipton, C.H.F. Peden, J. Szanyi, Angew. Chem. 125 (2013) 10169–10173.
[32] J. Wang, T. Yu, X. Wang, G. Qi, J. Xue, M. Shen, W. Li, Appl. Catal. B: Environ. 127 (2012) 137–147.
[33] H. Zhu, J.H. Kwak, C.H.F. Peden, J. Szanyi, Catal. Today 205 (2013) 16–23.
[34] D. Wang, L. Zhang, K. Kamasamudram, W.S. Epling, ACS Catal. 3 (2013) 871–881.
[35] J. Szanyi, J.H. Kwak, H. Zhu, C.H.F. Peden, Phys. Chem. Chem. Phys. 15 (2013) 2368–2380.
[36] J.H. Kwak, D. Tran, S.D. Burton, J. Szanyi, J.H. Lee, C.H.F. Peden, J. Catal. 287 (2012) 203–209.
[37] L. Ma, Y. Cheng, G. Cavataio, R.W. McCabe, L. Fu, J. Li, Chem. Eng. J. 225 (2013) 323–330.
[38] Y.J. Kim, J.K. Lee, K.M. Min, S.B. Hong, I.-S. Nam, B.K. Cho, J. Catal. 311 (2014) 447–457.
[39] I. Lezcano-Gonzalez, U. Deka, B. Arstad, A. Van Yperen-De Deyne, K. Hemelsoet, M. Waroquier, V. Van Speybroeck, B.M. Weckhuysen, A.M. Beale, Phys. Chem. Chem. Phys. 16 (2014) 1639–1650.
[40] F. Gao, J. Kwak, J. Szanyi, C.F. Peden, Top. Catal. 56 (2013) 1441–1459.
[41] R.Q. Long, R.T. Yang, J. Catal. 198 (2001) 20–28.
[42] X. Chen, W. Li, J.W. Schwank, Catal. Today 175 (2011) 2–11.
[43] M. Colombo, I. Nova, E. Tronconi, Catal. Today 197 (2012) 243–255.
[44] J. Dedecek, Z. Sobalik, Z. Tvaruazkova, D. Kaucky, B. Wichterlova, J. Phys. Chem. 99 (1995) 16327–16337.
[45] Y. Kuroda, R. Kumashiro, T. Yoshimoto, M. Nagao, Phys. Chem. Chem. Phys. 1 (1999) 649–656.
[46] S. Kieger, G. Delahay, B. Coq, B. Neveu, J. Catal. 183 (1999) 267–280.
[47] G. Delahay, B. Coq, S. Kieger, B. Neveu, Catal. Today 54 (1999) 431–438.
[48] L. Ma, J. Li, R. Ke, L. Fu, J. Phys. Chem. C 115 (2011) 7603–7612.
[49] H. Sjovall, E. Fridell, R.J. Blint, L. Olsson, Top. Catal. 42-43 (2007) 113–117.
[50] A. Zecchina, L. Marchese, S. Bordiga, C. Pazè, E. Gianotti, J. Phys. Chem. B 101 (1997) 10128–10135.
[51] L.J. Lobree, I.-C. Hwang, J.A. Reimer, A.T. Bell, J. Catal. 186 (1999) 242–253.
[52] K.I. Hadjiivanov, Catal. Rev. Sci. Eng. 42 (2000) 71–144.
[53] M. Iwasaki, K. Yamazaki, K. Banno, H. Shinjoh, J. Catal. 260 (2008) 205–216.
[54] R.Q. Long, R.T. Yang, J. Catal. 207 (2002) 224–231.
[55] J. Eng, C.H. Bartholomew, J. Catal. 171 (1997) 27–44.
[56] P.S. Metkar, V. Balakotaiah, M.P. Harold, Catal. Today 184 (2012) 115–128.
[57] L. Lisi, R. Pirone, G. Russo, N. Santamaria, V. Stanzione, Appl. Catal. A-Gen. 413 (2012) 117–131.
[58] S. Brandenberger, O. Kröcher, A. Tissler, R. Althoff, Catal. Rev.: Sci. Eng. 50 (2008) 492–531.